Customized Scheduling of Demand Response of Customers with Dispatchable Inverters in Distribution-level Photovoltaic Facilities

Lester Marrero, Daniel Sbárbaro, *Senior Member*, *IEEE*, and Luis García-Santander

***Abstract*—The growing electricity demand, combined with the increasing integration of photovoltaic (PV) generation into the distribution system, requires higher flexibility from the demand side. This paper proposes a customized scheduling approach for demand response (DR) of customers with dispatchable inverters in distribution-level PV facilities. Based on the Chilean context, the proposed approach enables these energy resources to provide flexibility in the technical and economic management of the distribution system operator (DSO). Specifically, a bi-level optimization model is introduced. At the upper level, the DSO minimizes distribution system costs by determining daily price signals for customers based on their response profile classes (RPCs) and active and reactive power set points for PV facilities. At the lower level, customers aim to reduce their electricity bills. In addition, the proposed approach ensures the reliable operation of the distribution system with high probability by addressing uncertainty through chance constraints (CCs). Incorporated CCs in the distribution system modeling include the squared magnitude of nodal voltage, complex power flow in lines, and apparent power of inverters. Finally, two case studies are presented, involving 420 residential and commercial Chilean customers with two distribution-level PV facilities using real-world market prices and daily consumption profiles on the IEEE 37-node test feeder. Results demonstrate how the proposed model enables the customized scheduling of customers and PV facilities, highlighting its effectiveness over the uniform price scheme.**

***Index Terms*—Scheduling, demand response (DR), inverter, distribution system, photovoltaic (PV), response profile class (RPC), uncertainty.**

I. Introduction

THE marked growth in electricity demand, driven mainly by emerging technologies such as electric vehicles and heat pumps, poses a significant challenge to the distribution system concerning electrification. In Chile, for example, the electricity consumption among residential and commercial customers and services in 2023 increased by 5.9% compared with 2022 and 10.2% compared with 2021 [1]. Also, the effective integration of renewable energy sources, especially photovoltaic (PV), into the distribution system remains problematic due to power balance issues. Both conditions need higher flexibility from the demand side, which can be achieved through demand response (DR).

The implementation of DR targets the control of the power-consuming behavior of customers to meet the following objectives: ① reduction of the peak power consumption; ② reduction of the total needed power generation, as the main result of the prior objective; ③ change of the demand to follow the available supply, especially with high penetration of renewable energy sources; and ④ elimination of overloads in the distribution system [2]. In particular, time-varying pricing, or dynamic pricing, can induce the DR of customers, thereby improving economic efficiency and enhancing welfare compared to other forms [3].

In this context, several investigations have attempted to determine effective time-varying price signals for customers by exploiting important mathematical programming models. Furthermore, these investigations can be classified based on the designed price signal. On the one hand, some of them determine a uniform price signal for the set of customers; on the other hand, others define customized pricing approaches for different groups of customers. In the former, for example, [4] analyzes the scheduling of the load-serving entity and formulates its interaction with flexible and inflexible aggregated loads as a bi-level problem that delivers hourly tariffs for the flexible ones. Reference [5] proposes a stochastic bi-level model in which the load-serving entity aims to optimize profit and reserve capacity and similarly designs dynamic prices for the aggregated flexible loads. Reference [6] formulates a hierarchical structure including the distribution system operator (DSO), DR providers, and customers, where dynamic and static prices are developed respectively for the flexible and inflexible customers. A stochastic scheduling approach is introduced in [7] to determine both the hourly retail prices considering the electricity value and the bidding strategy of the distribution company in the day-ahead mar-

Manuscript received: December 6, 2024; revised: March 12, 2025; accepted: May 20, 2025. Date of CrossCheck: May 20, 2025. Date of online publication: June 11, 2025.

This work was supported in part by the National Agency for Research and Development under Grant ANID-PFCHA/Doctorado Nacional/21202246 and the FONDAP Project 15110019.

L. Marrero (corresponding author) is with the Center for Energy Transition (CENTRA), Universidad Adolfo Ibáñez, Santiago 7941169, Chile (e-mail: lester.marrero@edu.uai.cl).

D. Sbárbaro and L. García-Santander are with the Department of Electrical Engineering, Universidad de Concepción, Concepción 4070409, Chile (e-mail: dsbarbar@udec.cl; luigarci@udec.cl).

DOI: 10.35833/MPCE.2024.001304

ket. In [8], a bi-level model that formulates the interaction between the DSO and end-users allows for the design of tariffs including uncertainty in demand, PV generation, and market prices. Reference [9] presents a dynamic pricing model to promote renewable integration and flatten the grid demand profile using a bi-level optimization that coordinately dispatches flexible loads. Based on the potential in DR of thermostatically controlled loads, [10] proposes a multi-perspective pricing model to formulate proper price signals. Lastly, a stochastic bi-level model is proposed in [11] to design daily retail prices for energy management of thermal loads in a community of buildings. Although these investigations make a notable effort by producing dynamic price signals and providing financial profits, their main limitation is considering the same price signal for customers with different preferences.

In line with this work, some studies have recently expanded the prior approach by introducing customized price signals. Reference [12] proposes a dynamic pricing method that includes adaptive customer segmentation and customized modeling of the resulting demand clusters based on aggregated price responses. However, the paper assumes a linear function for the price elasticities of demand. This approximation requires many observations to estimate the corresponding parameters, which contrasts with the ideal case of daily segmentation. Assuming different types of flexible consumers, [13] presents a bi-level optimization for customized retail pricing and bidding of the aggregated demand in the day-ahead market. Through a bi-level model, [14] determines customized retail prices for groups of residential and industrial consumers, considering a price-elastic demand for the first and learning the price-demand relation for the second. However, a practical limitation for the groups of residential consumers is obtaining the actual proportions of the shiftable and curtailable loads. The common point among these papers is the generation of daily price signals based on the characteristics of customer groups. However, two key research questions that motivate this investigation remain unanswered. ① Is it feasible to determine the price signals that provide desired power responses from customers according to the conditions of the distribution system? ② How can the uncertainty associated with customers' behavior be accounted for? Answering both questions requires the individual characterization of customers and assessing the impact of their consumption profiles on the distribution system in response to the customized tariffs while also considering deviations from expected behaviors.

Furthermore, the increasing distribution-level PV generation raises the interest in scheduling the operation of inverters to provide active power and control reactive power. In Chile, by March 2025, the capacity of this type of distributed generation is 2833 MW [15]. The implementation of optimization techniques that include computing the power set points of dispatchable inverters in PV facilities has also been developed based on forecasts of available generation and the expected behavior of customers. Among the related works, [16] introduces a chance-constrained AC power flow where the power set points for PV and battery systems are optimized while enforcing voltage regulation with uncertainty in renewable energy sources and loads. Similarly, [17] enables the DSO to obtain the dispatch for PV and battery systems using a chance-constrained model that accounts for uncertainty in PV generation, end-user consumption, requested flexibility, and squared voltage magnitude. Considering the uncertainty of PV generation, [18] formulates a robust optimization that selects the critical subset of inverters to provide ancillary services and finds their optimal active and reactive power set points. The above studies focus on determining the optimal power set points of inverters, primarily for local voltage regulation; however, they do not intend to control DR.

By appropriately choosing dynamic price signals, the DSO reduces distribution system costs and increases reliability, for example, by shifting flexible consumption to periods with high stochastic power generation [19]. This paper presents a daily scheduling approach for DR of customers through customized price signals and dispatchable inverters in distribution-level PV facilities. To this end, a bi-level optimization model [20] is introduced with the DSO at the upper level and customers at the lower level. The DSO minimizes costs and determines the customized price signals and power set points of inverters, while customers reduce their electricity bills when the prices materialize. This paper comprises a characterization stage to determine response profile classes (RPCs) [21] of customers and assesses the impact of their power responses on the distribution system. The proposed model also addresses the uncertainty in the distribution-system modeling by including chance constraints (CCs) [22] for the squared magnitude of nodal voltage, complex power flow in lines, and apparent power of inverters. By assuming a normal distribution for uncertainty, the CCs are then analytically reformulated. Lastly, with the reformulation of lower-level problems, the chance-constrained bi-level model is converted to an equivalent mixed-integer second-order cone programming (MISOCP) model.

The ongoing electrification of the Chilean residential and commercial sectors requires additional infrastructure in the distribution system. In general, end-users are responsible for covering the associated costs. However, exploiting demand-side flexibility contributes to avoiding (or delaying) the operational cost increase and need for new investments, thus facilitating the electrification. Regulated customers in Chile typically contract a (regulated) tariff of a single energy price. However, the DSO, which obtains electricity through bilateral contracts, can offer additional tariff options (the regulated flexible tariffs) [23], which remain valid for 12 months and may include dynamic pricing. This paper explores a scenario in which the DSO engages with customers using this type of flexible tariff.

The main contributions of this paper are summarized below.

1) A daily scheduling approach is proposed for DR of customers through customized price signals and dispatchable inverters in distribution-level PV facilities based on the condi-

tions of the distribution system. This study determines the RPCs of customers and assesses the impact of their consumption profiles on the distribution system in response to the customized price signals. In addition, uncertainty is addressed in the distribution-system modeling considering the stochastic nature of customers and PV generation. A chance-constrained bi-level programming model is introduced with the DSO at the upper level and customers at the lower level. The DSO minimizes distribution-system costs by determining the price signals and power set points such that limits of squared magnitudes of nodal voltages, complex power flows in lines, and apparent power of inverters are satisfied with high probability. Customers aim to reduce their electricity bills.

2) The proposed approach is tested in two case studies with real-world market prices and daily consumption profiles of residential and commercial Chilean customers on the IEEE 37-node test feeder. Results demonstrate how the proposed model enables the customized scheduling of customers and PV facilities. This paper also explores the impact of uncertainty on grid operation and presents a comparison with the uniform price scheme.

The organization of this paper is as follows: Section II provides theoretical foundations and models for customers, PV facilities, and the distribution system. Section III formulates the programming problem under uncertainty, and Section IV describes its solution methodology. Section V presents the case studies to assess the proposed approach and analyze the uncertainty cost. Finally, Section VI concludes the work.

II. Theoretical Foundations and Models

A. Expected Response Model of Customers

Let $\bar{s}_{l_t}=\bar{p}_{l_t}+\mathrm{j}\bar{q}_{l_t}$ be an expected complex power value to be consumed at time t by a customer l under a contract. Therefore, $\bar{p}_{l_t}$ is the active component and $\bar{q}_{l_t}$ is the reactive one. In this paper, the following linear model is defined to set a flexible active power profile [19]:

$$p_{l_t}^{\min}\le\bar{p}_{l_t}:\beta_{l_t}^{\min}\quad l\in L,t\in T \tag{1}$$

$$\bar{p}_{l_t}\le p_{l_t}^{\max}:\beta_{l_t}^{\max}\quad l\in L,t\in T \tag{2}$$

$$\sum_{t=1}^{T}\bar{p}_{l_t}\Delta t\ge e_l:\varepsilon_l\quad l\in L \tag{3}$$

Equations (l) and (2) provide the expected response $\bar{p}_{l_t}$ between a minimum value $p_{l_t}^{\min}$ and a maximum value $p_{l_t}^{\max}$ for customer l at time t, as an element of its expected active power profile. Likewise, L and T are the sets of customers and time points within the day, respectively. Also, $\bar{p}_{l_t}$ can increase or decrease depending on the price due to the combined use of shifting and shedding loads. From an expected value $\bar{p}_{l_t}$, the corresponding expected response $\bar{q}_{l_t}$ can be obtained for a specific power factor. Finally, a minimum daily energy e_l is specified by (3) to account for basic activities, where Δt is the interval between two consecutive time points. Variables $\beta_{l_t}^{\min}$, $\beta_{l_t}^{\max}$, and ε_l, arranged after the colon, are dual.

A refined estimation of the customer's consumption activity is feasible based on an online characterization of daily consumption profiles, as demonstrated in [21], which presents the customer's RPCs (or consumption patterns) as the main result. Each RPC represents for a customer a portion (of similar daily consumption profiles) of the polytope that entirely contains its load scenarios in the corresponding vector space. Similarly, this paper comprises a characterization stage. Specifically, it applies the clustering by fast search and find of density peaks (CFSFDP) algorithm [24] directly to the daily consumption profiles of a predefined period before a selected date for the proposed approach, resulting in updated customers' RPCs. For the above-selected date, this paper assumes that customers use the highest-probability RPC on the day of the week corresponding to that date.

From a set of daily consumption profiles associated with a specific RPC, each pair of parameters $p_{l_t}^{\min}$ and $p_{l_t}^{\max}$ of the model can be obtained as the corresponding extreme values, providing a convex approximation of the active power. For e_l, this paper considers the total consumption of the average profile among all profiles within the RPC.

B. Model of PV Facilities

Let $\bar{s}_{g_t}=\bar{p}_{g_t}+\mathrm{j}\bar{q}_{g_t}$ be a complex power forecast to be injected by a PV facility $g\in G$ at time t, where G is the set of PV facilities. Therefore, $\bar{p}_{g_t}$ is the active component, which represents the active power forecast at the AC side of the inverter, and $\bar{q}_{g_t}$ is the reactive one. Then, the following control model is defined for setting a flexible active power profile:

$$0\le\bar{p}_{g_t}\le\bar{p}_{g_t}^{av}\quad g\in G,t\in T \tag{4}$$

Equation (4) denotes an active power curtailment provided by the inverter, where $\bar{p}_{g_t}^{av}$ is the forecast of the available active power, which coincides with the maximum power point and varies stochastically over time based on solar irradiance.

With the increasing penetration of distribution-level PV facilities, interest is shifting toward using inverter capability to absorb or inject reactive power. In addition to (4), the following constraint defines the inverter capability for adjusting the reactive power output:

$$\bar{p}_{g_t}^2+\bar{q}_{g_t}^2\le(S_g^{\max})^2\quad g\in G,t\in T \tag{5}$$

where $S_g^{\max}$ is the rated apparent power of the inverter of PV facility g.

However, the IEEE Standard 1547-2018 [25] encourages the inverter-level modulation of power values in response to local grid conditions. This standard recommends injecting or absorbing reactive power for active power output levels greater than or equal to the minimum steady-state active power capability. As a result, the convex region defined from this value in the complex plane entitles reactive power generation exclusively during daylight.

C. Model of Distribution System

This paper uses the linear DistFlow model introduced by [26], which is a lossless approximation of the AC power flow equations. The approximate relations to account for power flows and nodal voltages in the distribution system facilitate the application of convex reformulations for CCs.

Let a radial distribution system comprise the corresponding nodes, collected in the set $N \cup \{0\}$ with N representing the set of nodes, and distribution lines, represented by the set of pairs of nodes $E = \{(m,n) : m \in N \cup \{0\}, n \in N\}$. Any sending node m lies on the unique path from node 0 to its receiving node n. Node 0 represents the secondary side of the power transformer at the substation and is considered as the slack node. Thus, its nominal voltage v_0 is fixed and known (typically 1.0 p.u.).

The power injection at slack node 0 depends on the power states of the other nodes. Each node n is characterized at time t by its complex power $S_{n_t} = P_{n_t} + \mathrm{j}Q_{n_t}$, where P_{n_t} and Q_{n_t} are the active and reactive power, respectively, and by the magnitude of its complex voltage v_{n_t}. To provide linear constraints, let V_{n_t} be the square of v_{n_t}. $V_{n_t} \in [V^{\min}, V^{\max}]$, where $V^{\min}$ and $V^{\max}$ are the minimum and maximum voltage limits, respectively. Likewise, each line (m,n) has an impedance value $Z_{mn} = R_{mn} + \mathrm{j}X_{mn}$, with R_{mn} and X_{mn} representing the resistance and reactance, respectively. Also, let $S_{mn_t} = P_{mn_t} + \mathrm{j}Q_{mn_t}$ denote the complex power flow from node m to node n at time t, where P_{mn_t} and Q_{mn_t} are the active and reactive power flows, respectively. Finally, let $S_{mn}^{\max}$ be the apparent power limit of the line.

From the above parameters, the following linear power flow and voltage equations are defined for the model:

$$P_{mn_t} = \boldsymbol{d}_{mn}^{\mathrm{T}} \boldsymbol{p}_t^n \quad (m,n) \in E, t \in T \tag{6}$$

$$Q_{mn_t} = \boldsymbol{d}_{mn}^{\mathrm{T}} \boldsymbol{q}_t^n \quad (m,n) \in E, t \in T \tag{7}$$

$$V_{n_t} = V_{m_t} - 2\left(R_{mn} P_{mn_t} + X_{mn} Q_{mn_t}\right) \quad (m,n) \in E, t \in T \tag{8}$$

where $\boldsymbol{d}_{mn}$ is a vector whose elements correspond to the $(m,n)^{\text{th}}$ row of a $|E| \times |N|$ binary matrix $\boldsymbol{D}$ that maps the values of active and reactive power at nodes into power flows and voltages, and $|\cdot|$ denotes the cardinality of a set; and $\boldsymbol{p}_t^n = \left[P_{1_t}, P_{2_t}, \ldots, P_{N_t}\right]^{\mathrm{T}}$ and $\boldsymbol{q}_t^n = \left[Q_{1_t}, Q_{2_t}, \ldots, Q_{N_t}\right]^{\mathrm{T}}$ are the vectors of active and reactive power of nodes, respectively. In $\boldsymbol{D}$, each element in the $(m,n)^{\text{th}}$ row and n^{th} column takes a value of 1 if line (m,n) is part of the path from the slack node 0 to node n and a value of 0 otherwise.

The expressions for the (net) active and reactive power at each node are as follows:

$$P_{n_t} = \boldsymbol{h}_n^{\mathrm{T}} \boldsymbol{p}_t \quad n \in N, t \in T \tag{9}$$

$$Q_{n_t} = \boldsymbol{h}_n^{\mathrm{T}} \boldsymbol{q}_t \quad n \in N, t \in T \tag{10}$$

where $\boldsymbol{h}_n$ is a vector whose elements correspond to the n^{th} column of an $|L+G| \times |N|$ binary matrix $\boldsymbol{H}$ that indicates the belonging of each customer l and PV facility g to the corresponding node n; and $\boldsymbol{p}_t$ and $\boldsymbol{q}_t$ are the vectors comprising active and reactive power of both customers and PV facilities at time t, respectively.

III. Programming Problem Formulation Under Uncertainty

A. Uncertainty Modeling

The modeling of active power values of customers and PV facilities can take the following form:

$$p_{l_t} = \bar{p}_{l_t} + \xi_{l_t} \quad l \in L, t \in T \tag{11}$$

$$p_{g_t} = \bar{p}_{g_t} + \xi_{g_t} \quad g \in G, t \in T \tag{12}$$

where $\xi_{l_t} \in \mathbb{R}$ and $\xi_{g_t} \in \mathbb{R}$ are the stochastic variables representing the deviation of customer response and the PV forecast error, respectively.

Thus, for each time t, a random vector $\boldsymbol{\xi}_t \in \mathbb{R}^N$ that collects the resulting active power deviation and forecast error at the nodes can be determined. Also, it is possible to express the power flows in lines and nodal voltages in terms of $\boldsymbol{\xi}_t$. For the first case:

$$P_{mn_t} = \bar{P}_{mn_t} + \boldsymbol{d}_{mn}^{\mathrm{T}} \boldsymbol{\xi}_t \quad (m,n) \in E, t \in T \tag{13}$$

$$Q_{mn_t} = \bar{Q}_{mn_t} + \boldsymbol{d}_{mn}^{\mathrm{T}} \boldsymbol{\Theta}_t \boldsymbol{\xi}_t \quad (m,n) \in E, t \in T \tag{14}$$

where $\bar{P}_{mn_t}$ and $\bar{Q}_{mn_t}$ are computed using (6) and (7) with expected and forecast values, respectively; and $\boldsymbol{\Theta}_t$ is an $|N| \times |N|$ diagonal matrix relating the active and reactive nodal deviations and errors through the tangent of the power factor angle at time t.

Analogously, the uncertain nodal voltages are:

$$V_{n_t} = \bar{V}_{n_t} - 2\boldsymbol{d}_n^{\mathrm{T}}\left(\boldsymbol{RD} + \boldsymbol{XD\Theta}_t\right)\boldsymbol{\xi}_t \quad n \in N, t \in T \tag{15}$$

where $\bar{V}_{n_t}$ is computed using (8) with expected and forecast values; $\boldsymbol{d}_n$ is a vector whose elements correspond to the n^{th} column of $\boldsymbol{D}$; and $\boldsymbol{R}$ and $\boldsymbol{X}$ are the $|N| \times |N|$ diagonal matrices with resistance and reactance values of lines, respectively.

B. Chance-constrained Bi-level Formulation

This paper presents a hierarchical programming structure comprising two levels to solve the daily scheduling problem. At the upper level, the DSO determines the price signals under uncertainty (for the selected date). At the lower level, each customer adjusts its consumption to reduce the electricity bill.

The objective function in (16a), representing the difference between cost and revenue for the DSO, is minimized under the expected value over the probability distribution of uncertainty. Each λ_{l_t} is a decision price, and λ_t^m is the market price. The operator $\mathbb{E}[\cdot]$ denotes the expected value. Equation (16b) defines a feasible region for the decision prices between a minimum value $\lambda^{\min}$ and a maximum value $\lambda^{\max}$. In (16c), the mean of prices λ_{l_t} over the time horizon T does not surpass the regulated price λ^r, which implies that customers do not incur financial losses beyond λ^r. The outer approximation set of CCs in (16d)-(16f) ensures that scheduling DR of customers and power set points of inverters satisfies the limits for squared magnitudes of nodal voltages, complex power flows in lines, and apparent power of inverters

with high probability, where ϵ_v, ϵ_f, and ϵ_a denote the corresponding violation probabilities, and the operator $\mathbb{P}\{\cdot\}$ denotes the probability distribution.

$$\min_{\lambda_{l_t},\bar{p}_{g_t},\bar{q}_{g_t},\bar{p}_{l_t}} \mathbb{E}\left[\sum_{t=1}^{T}\lambda_t^m\left(\sum_{l=1}^{L}p_{l_t}-\sum_{g=1}^{G}p_{g_t}\right)\Delta t-\sum_{t=1}^{T}\sum_{l=1}^{L}\lambda_{l_t}p_{l_t}\Delta t\right] \tag{16a}$$

s.t.

$$\lambda^{\min}\le\lambda_{l_t}\le\lambda^{\max}\quad l\in L,t\in T \tag{16b}$$

$$\frac{1}{T}\sum_{t=1}^{T}\lambda_{l_t}\le\lambda^{r}\quad l\in L \tag{16c}$$

$$\mathbb{P}\left\{V^{\min}\le V_{n_t}\le V^{\max}\right\}\ge 1-\epsilon_v\quad n\in N,t\in T \tag{16d}$$

$$\mathbb{P}\left\{P_{mn_t}^2+Q_{mn_t}^2\le\left(S_{mn}^{\max}\right)^2\right\}\ge 1-\epsilon_f\quad (m,n)\in E,t\in T \tag{16e}$$

$$\mathbb{P}\left\{p_{g_t}^2+q_{g_t}^2\le\left(S_{g}^{\max}\right)^2\right\}\ge 1-\epsilon_a\quad g\in G,t\in T \tag{16f}$$

$$(4),\ (6)\text{-}(10) \tag{16g}$$

Equation (16h) represents the lower-level problems, which enforce the expected optimal response of customers given the decision prices λ_{l_t}.

$$\begin{cases}\bar{p}_{l_t}\in\ \arg\min\limits_{\bar{p}_{l_t}}\left(\sum\limits_{t=1}^{T}\lambda_{l_t}\bar{p}_{l_t}\Delta t\right)\quad l\in L\\ \text{s.t. (1)-(3)}\end{cases} \tag{16h}$$

IV. Problem Solution Methodology

Due to (16d)-(16f), the problem solution becomes computationally intractable. This section first provides second-order cone (SOC) reformulations for these CCs, assuming the DSO knows the probability density function of vectors $\boldsymbol{\xi}_t$. Specifically, each $\boldsymbol{\xi}_t\sim\mathcal{N}\left(0,\boldsymbol{\Sigma}_t\right)$, where $\mathcal{N}(\cdot)$ represents the normal distribution function, and $\boldsymbol{\Sigma}_t\in\mathbb{R}^{N\times N}$ is a diagonal matrix. Furthermore, due to (16h), tractability depends on reformulating the problem into a single-level one. Since prices λ_{l_t} are parameters in the lower-level problems, their objective functions and corresponding constraints are linear in the decision variables $\bar{p}_{l_t}$. Thus, the Karush-Kuhn-Tucker (KKT) optimality conditions [27], which are necessary and sufficient for global optimality, can be used in their place. Finally, the objective function includes bilinear products, which introduce nonlinearity. However, this nonlinearity can be addressed through linearization using duality theory [27].

A. Reformulation of CCs

1) Voltage CCs. Every single constraint in (16d) with a limit for the squared magnitude of nodal voltage is a CC of the general form: $\mathbb{P}\left\{a+\boldsymbol{b}^{\mathrm{T}}\boldsymbol{\xi}_t\le c\right\}\ge 1-\epsilon$, where $a\in\mathbb{R}$ is the nominal squared voltage; $\boldsymbol{b}\in\mathbb{R}^N$ denotes the influence of $\boldsymbol{\xi}_t$ on the constraint; c is a constant representing the voltage limit; and ϵ is the violation probability. In particular, the left-hand side is a random variable whose distribution denotes the variations in the corresponding voltage, with mean a and standard deviation $\left\|\boldsymbol{b}^{\mathrm{T}}\boldsymbol{\Sigma}_t^{1/2}\right\|_2$. The CC is reformulated exactly into the following SOC constraint: $a\le c-\Phi^{-1}(1-\epsilon)\left\|\boldsymbol{b}^{\mathrm{T}}\boldsymbol{\Sigma}_t^{1/2}\right\|_2$, where Φ is the cumulative distribution function (CDF) of the standard normal distribution. Thus, CCs of squared magnitudes of nodal voltages in (16d) can be rewritten as:

$$\bar{V}_{n_t}\le V^{\max}-2\Phi^{-1}\left(1-\epsilon_v\right)\left\|\boldsymbol{d}_n^{\mathrm{T}}\left(\boldsymbol{RD}+\boldsymbol{XD\Theta}_t\right)\boldsymbol{\Sigma}_t^{1/2}\right\|_2\quad n\in N,t\in T \tag{17a}$$

$$-\bar{V}_{n_t}\le -V^{\min}-2\Phi^{-1}\left(1-\epsilon_v\right)\left\|\boldsymbol{d}_n^{\mathrm{T}}\left(\boldsymbol{RD}+\boldsymbol{XD\Theta}_t\right)\boldsymbol{\Sigma}_t^{1/2}\right\|_2\quad n\in N,t\in T \tag{17b}$$

2) Power flow CCs. Every single constraint in (16e) with a limit for the magnitude of complex power flow is a CC of the general form: $\mathbb{P}\left\{\left(a_1+\boldsymbol{b}_1^{\mathrm{T}}\boldsymbol{\xi}_t\right)^2+\left(a_2+\boldsymbol{b}_2^{\mathrm{T}}\boldsymbol{\xi}_t\right)^2\le c^2\right\}\ge 1-\epsilon$, where $a_1,a_2\in\mathbb{R}$ are the nominal active and reactive power flows in the line, respectively; $\boldsymbol{b}_1,\boldsymbol{b}_2\in\mathbb{R}^N$ denote the corresponding influence of $\boldsymbol{\xi}_t$; and c is a constant representing the apparent power limit in this general form. The two terms on the left-hand side are squared random variables that denote the operating points of the active and reactive power flows, respectively, contained in the region $\mathcal{S}\in\mathbb{R}^2$. $\mathcal{S}$ is convex and can be internally approximated by the I-sided polygon $\mathcal{P}$ inscribed inside $\mathcal{S}$, with I even and selected in advance [28]. Then, this paper defines that $\mathcal{P}=\{\boldsymbol{Ws}\le\boldsymbol{0}\}$, where $\{\boldsymbol{Ws}\le\boldsymbol{0}\}$ is a set of half-space linear constraints; $\boldsymbol{W}$ is an $I\times 3$ matrix of coefficients; and $\boldsymbol{s}\in\mathbb{R}^3$ is the vector formed by each of the elements of the above general form. By expressing the coefficients of any i^{th} row of $\boldsymbol{W}$ as $w_{i,1}$, $w_{i,2}$, and $w_{i,3}$, the following linear CC results are obtained for $i=1,2,\ldots,I$: $\mathbb{P}\left\{w_{i,1}\left(a_1+\boldsymbol{b}_1^{\mathrm{T}}\boldsymbol{\xi}_t\right)+w_{i,2}\left(a_2+\boldsymbol{b}_2^{\mathrm{T}}\boldsymbol{\xi}_t\right)+w_{i,3}c\le 0\right\}\ge 1-\epsilon$. Due to $\boldsymbol{\xi}_t$ in both random variables, the following set of constraints for the half-space approximation of $\mathcal{S}$ can replace the CCs of complex power flows in (16e):

$$\begin{aligned}w_{i,1}\bar{P}_{mn_t}+w_{i,2}\bar{Q}_{mn_t}\le&-w_{i,3}S_{mn}^{\max}-\\&\Phi^{-1}\left(1-\epsilon_f\right)\left\|\left[w_{i,1}\boldsymbol{d}_{mn}^{\mathrm{T}}+w_{i,2}\boldsymbol{d}_{mn}^{\mathrm{T}}\boldsymbol{\Theta}_t\right]\boldsymbol{\Sigma}_t^{1/2}\right\|_2\\&i=1,2,\ldots,I,(m,n)\in E,t\in T\end{aligned} \tag{18}$$

3) Apparent power CCs. Every single constraint in (16f) with a limit for the inverter capacity is a CC of the general form: $\mathbb{P}\left\{\left(a_1+\xi_{g_t}\right)^2+a_2^2\le c^2\right\}\ge 1-\epsilon$, where in this general form, $a_1,a_2\in\mathbb{R}$ are the nominal active and reactive power of the inverter, respectively; and c is a constant representing its apparent power limit. The squared random variable and the squared scalar variable, on the left-hand side, denote respectively the operating points of the active and reactive power contained in the region $\mathcal{S}\in\mathbb{R}^2$. As in the above situation, $\mathcal{S}$ is convex and can be internally approximated by the I-sided polygon $\mathcal{P}$ inscribed inside $\mathcal{S}$. By expanding on this, the following linear CC can be obtained as: $\mathbb{P}\left\{w_{i,1}\left(a_1+\xi_{g_t}\right)+w_{i,2}a_2+w_{i,3}c\le 0\right\}\ge 1-\epsilon,\forall i,w_{i,1}\ge 0$. Thus, the following set of constraints for the half-space approximation of $\mathcal{S}$ can replace the CCs of active and reactive power set points of in-

verters in (16g):

$$w_{i,1}\bar{p}_{g_t}+w_{i,2}\bar{q}_{g_t}\le -w_{i,3}S_g^{\max}-\Phi^{-1}(1-\epsilon_a)\left\|w_{i,1}\sigma_{g_t}\right\|_2 \quad \forall i, w_{i,1}\ge 0, g\in G, t\in T \tag{19}$$

where σ_{g_t} is the standard deviation of forecast errors for PV facility g at time t.

B. Reformulation of Lower-level Problems

The following expressions are obtained by applying the KKT formulation to the lower-level problems:

$$\Delta t\lambda_{l_t}-\beta_{l_t}^{\min}+\beta_{l_t}^{\max}-\varepsilon_l\Delta t=0 \quad l\in L, t\in T \tag{20a}$$

$$0\le \beta_{l_t}^{\min}\perp \bar{p}_{l_t}-p_{l_t}^{\min}\ge 0 \quad l\in L, t\in T \tag{20b}$$

$$0\le \beta_{l_t}^{\max}\perp -\bar{p}_{l_t}+p_{l_t}^{\max}\ge 0 \quad l\in L, t\in T \tag{20c}$$

$$0\le \varepsilon_l\perp \sum_{t=1}^{T}\bar{p}_{l_t}\Delta t-e_l\ge 0 \quad l\in L \tag{20d}$$

Equation (20a) is the gradient of the Lagrange function concerning variables $\bar{p}_{l_t}$. Likewise, (20b)-(20d) represent the complementary slackness conditions between the non-negative dual variables and the inequality constraints of the primal problem. Due to the nonlinearity of complementary slackness conditions, the mixed-integer method of [29] is used, resulting in the following set of linear constraints:

$$0\le \beta_{l_t}^{\min}\le M^{\mathrm{d}}B_{l_t}^{\min} \quad l\in L, t\in T \tag{21a}$$

$$0\le \bar{p}_{l_t}-p_{l_t}^{\min}\le M^{\mathrm{p}}\left(1-B_{l_t}^{\min}\right) \quad l\in L, t\in T \tag{21b}$$

$$0\le \beta_{l_t}^{\max}\le M^{\mathrm{d}}B_{l_t}^{\max} \quad l\in L, t\in T \tag{21c}$$

$$0\le -\bar{p}_{l_t}+p_{l_t}^{\max}\le M^{\mathrm{p}}\left(1-B_{l_t}^{\max}\right) \quad l\in L, t\in T \tag{21d}$$

$$0\le \varepsilon_l\le M^{\mathrm{d}}E_l \quad l\in L \tag{21e}$$

$$0\le \sum_{t=1}^{T}\bar{p}_{l_t}\Delta t-e_l\le M^{\mathrm{p}}\left(1-E_l\right) \quad l\in L \tag{21f}$$

$$B_{l_t}^{\min}, B_{l_t}^{\max}\in\{0,1\} \quad l\in L, t\in T \tag{21g}$$

$$E_l\in\{0,1\} \quad l\in L \tag{21h}$$

where M^{p} and M^{d} are the positive constants that are valid as upper bounds for the primal and dual variables, respectively.

C. Reformulation of Objective Function

Bilinear products $\lambda_{l_t}\bar{p}_{l_t}$ in the objective function (16a) introduce nonlinearity. However, this bilinear term can be written in terms of the dual variables of the lower-level problems. The objective function of dual problems is derived by multiplying each dual variable by the constant on the right-hand side of its associated primal constraint and summing these products. Therefore, the following strong-duality equality is obtained:

$$\sum_{t=1}^{T}\lambda_{l_t}\bar{p}_{l_t}\Delta t=\sum_{t=1}^{T}\left(p_{l_t}^{\min}\beta_{l_t}^{\min}-p_{l_t}^{\max}\beta_{l_t}^{\max}\right)+e_l\varepsilon_l \quad l\in L \tag{22}$$

Finally, the chance-constrained bi-level problem converts to the equivalent MISOCP problem, where the optimal solution can be found through the branch and bound algorithm [27]:

$$\begin{cases}\min\limits_{\lambda_{l_t},\bar{p}_{g_t},\bar{q}_{g_t},\bar{p}_{l_t}} \mathbb{E}\left\{\left(\sum\limits_{t=1}^{T}\lambda_t^m\left(\sum\limits_{l=1}^{L}p_{l_t}-\sum\limits_{g=1}^{G}p_{g_t}\right)\Delta t-\sum\limits_{l=1}^{L}\left[\sum\limits_{t=1}^{T}\left(p_{l_t}^{\min}\beta_{l_t}^{\min}-p_{l_t}^{\max}\beta_{l_t}^{\max}\right)+e_l\varepsilon_l\right]\right\}\\ \text{s.t. (4), (6)-(10), (16b), (16c), (17a), (17b), (18), (19), (20a), (21a)-(21h)}\end{cases} \tag{23}$$

V. Case Studies

This section presents two case studies to demonstrate the benefits of the proposed approach and a comparison analysis with the uniform price scheme. In the algorithmic implementation, the toolbox YALMIP [30] on MATLAB 2022, with the Gurobi optimization solver, is used.

The case studies use a modified version of the IEEE 37-node test feeder [31], replacing the original spot loads with electricity data of 420 residential and commercial Chilean customers, which is shown in Fig. 1. It operates at 4.8 kV line-to-line nominal voltage. The measurement period for the two cases corresponds to three weeks: from February 14 to March 5 for the first case, and from February 21 to March 12 for the second case, both in 2020. Two PV facilities are added to the modified IEEE 37-node test feeder to emulate the penetration of renewable energy sources on the DSO scale. Table I outlines the (random) allocation of customers at load nodes and the nodes for PV generation. The test dates are March 6 and March 13, for which the local market prices at the customers' substation are used, while the PV generation profiles are simulated based on historical weather data [32] in their geographical area. Figure 2 depicts the PV generation and local market prices on the selected dates.

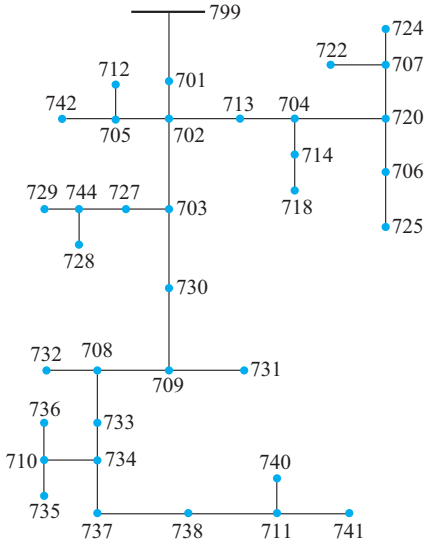

Fig. 1. Modified IEEE 37-node test feeder considered in case studies.

This paper also defines a feasible region for decision prices between 60 \$/MWh and 80 \$/MWh, with a regulated price of 75 \$/MWh. The violation probabilities in CCs are $\epsilon_v=0.1$, $\epsilon_f=0.01$, and $\epsilon_a=0.01$. Limits for nodal voltages are set to be 1.05 p.u. and 0.95 p.u., while for power flows, the

corresponding calculation uses the line-to-line nominal voltage and ampacity of electrical conductors. For the dispatchable inverters of PV facilities, $S_g^{\max}=370$ kVA, and the minimum steady-state active power capability is 7% of $S_g^{\max}$. The upper bounds in the lower-level problems are $M^{\mathrm{p}}=30$ and $M^{\mathrm{d}}=60$, while $I=12$ for the polygon $\mathcal{P}$.

TABLE I
ALLOCATION OF CUSTOMERS AT LOAD NODES AND NODES FOR PV GENERATION

Load node (number of customers)	Node for PV generation (number of PV facilities)
701 (71), 712 (11), 713 (9), 714 (5), 718 (11), 720 (14), 722 (24), 724 (6), 725 (7), 727 (6), 728 (21), 729 (9), 730 (16), 731 (16), 732 (9), 733 (18), 734 (9), 735 (22), 736 (9), 737 (32), 738 (32), 740 (19), 741 (25), 742 (13), 744 (6)	707 (1), 711 (1)

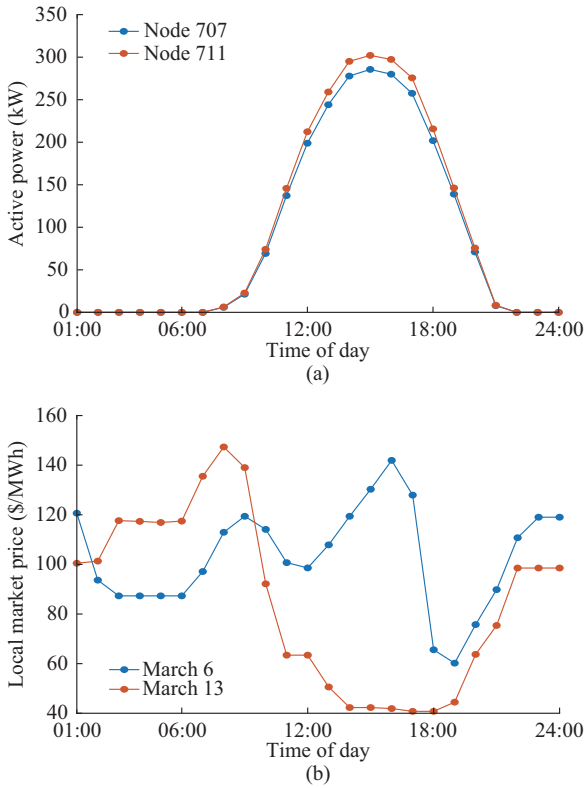

Fig. 2. PV generation and local market prices on March 6 and March 13. (a) PV generation. (b) Local market prices.

Lastly, to construct vectors $\boldsymbol{\xi}_t$, 90 samples are drawn from normal distributions of nodal demand deviations and forecast errors. To reflect the evolution of uncertainty over time, the standard deviation is assumed to be 3% of the expected or forecasted active power for the 1st and 2nd hours, 6% for the 3rd to 5th hours, 10% for the 6th to 9th hours, 15% for the 10th to 14th hours, and 20% for the rest of future time. The nodal expected or forecasted value considers the aggregated average demand or the available PV generation. Power factors of 0.93 and 0.86 are assumed for residential and commercial customers, respectively.

A. Case Study I

The application of the CFSFDP algorithm to the measurement results in three clusters. Their corresponding daily consumption profiles are depicted in Fig. 3, with cardinalities of 3279, 5141, and 288, respectively. The black profile represents the cluster center. Cluster 1 exhibits a typical residential pattern characterized by a slightly higher consumption at night. Cluster 2 presents a pattern where consumption is concentrated during working hours, suggesting that most commercial facilities and businesses are included. Instead, cluster 3 presents a pattern with lower consumption during daylight hours, likely because of vacations during this period.

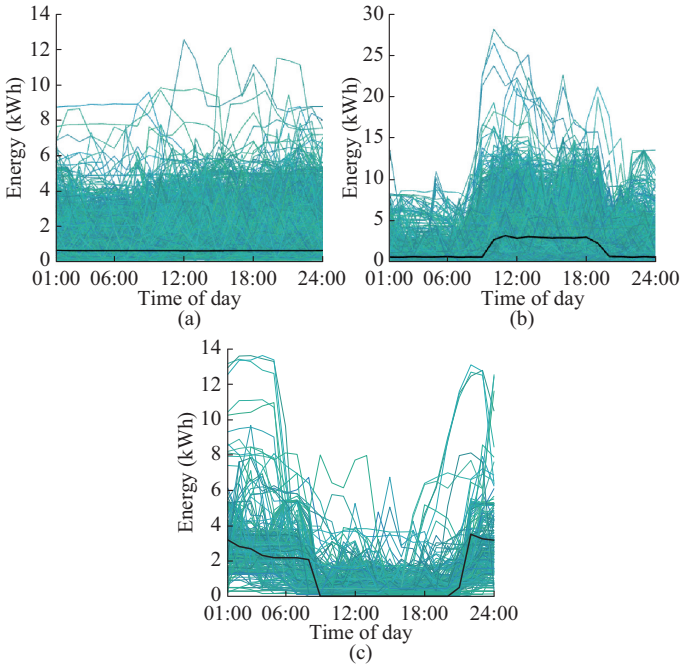

Fig. 3. Daily consumption profiles of three clusters. (a) Cluster 1. (b) Cluster 2. (c) Cluster 3.

Table II summarizes the RPCs, their combinations, and the number of customers per highest-probability RPC on March 6 (which results in the same three RPCs). Most consumers use two RPCs during the period, mainly a combination of RPCs 1 and 2 (71.7% of the total). Also, the DSO expects mostly the RPC 2, characterized by higher consumption values.

TABLE II
RPCS, THEIR COMBINATIONS, AND NUMBER OF CUSTOMERS PER HIGHEST-PROBABILITY RPC ON MARCH 6

RPC	Number of customers	Combination of RPCs (number of customers in corresponding combination)	Number of customers per highest-probability RPC on March 6
1	58	2 (40), 1 (15), 3 (3)	128
2	313	1-2 (301), 1-3 (8), 2-3 (4)	285
3	49	1-2-3 (49)	7

Figures 4 and 5 illustrate the three customized price signals to be broadcast by the DSO and the expected consumption profiles, respectively.

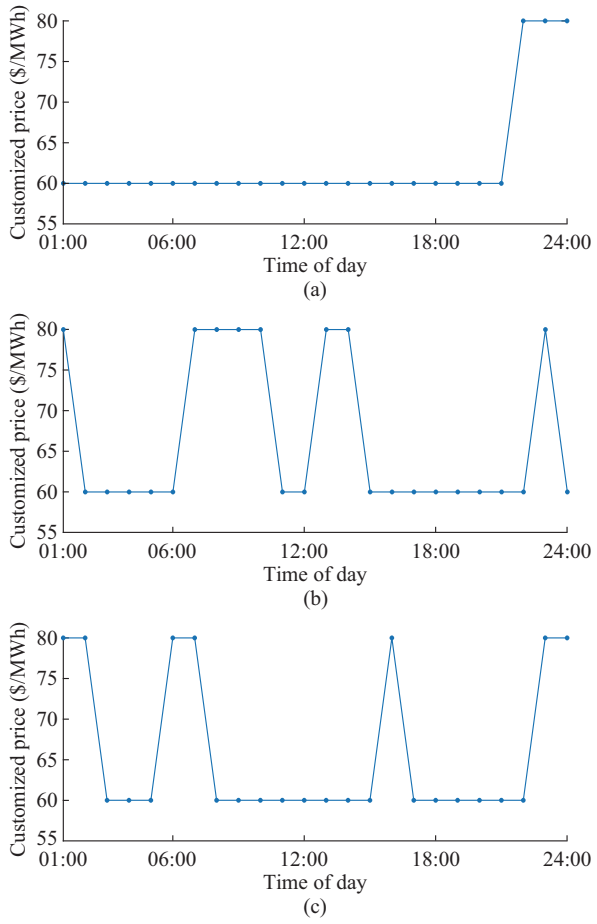

Fig. 4. Customized price signals according to highest-probability RPC on March 6. (a) RPC 1. (b) RPC 2. (c) RPC 3.

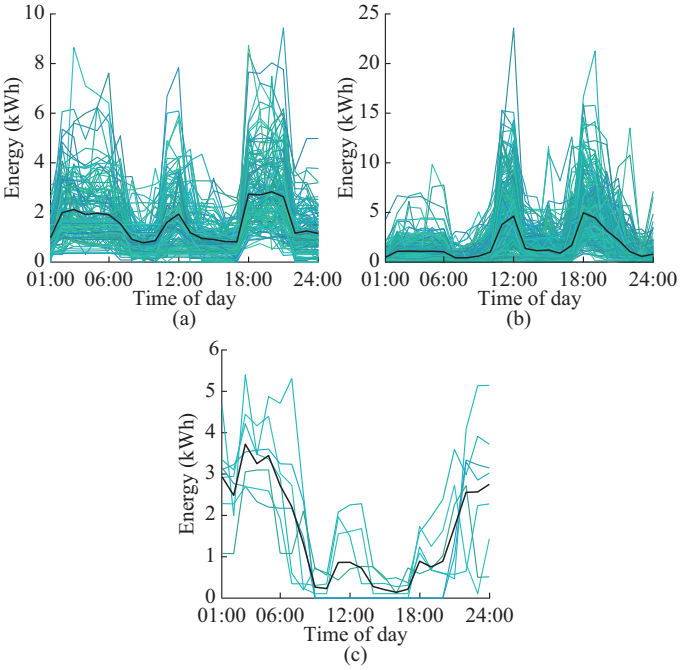

Fig. 5. Expected consumption profiles of customers on March 6. (a) RPC 1. (b) RPC 2. (c) RPC 3.

In Fig. 5, the black profile represents the average consumption. The customized price signal according to RPC 1 shows 60 $/MWh for almost the entire day, except for the last three hours when it increases to the maximum price. The consumption of customers with RPC 1 during these hours is also higher. Thus, the DSO's interest is for these customers to shift part of their consumption activities from this period to the rest of the day. Likewise, the customized price signal according to RPC 2 matches the shape of market prices very well, with a significant difference only in the peak prices from 15:00 to 17:00. This difference is because this period also coincides with the higher PV generation (15:00 corresponds to the maximum PV generation). Therefore, the DSO encourages customers with RPC 2 to shift intended consumption activities to this period and others with lower market prices. Customers with RPC 3 have the lowest influence compared with those with RPCs 1 and 2. The customized price signal, according to RPC 3, aims to shift consumption activities mainly to working hours, except at 16:00, when the market price is the highest.

As a result, customers with RPCs 1 and 2, due to their inherent flexibility, have higher consumption during periods with the minimum price (60 $/MWh). In contrast, customers with RPC 3 experience a slight increase in consumption around noon.

For the PV facilities, Fig. 6 depicts their active and reactive power set points at nodes 707 and 711. The active power output comprises some values below the available active power during the higher-generation period due to the consideration of the uncertainty. On the other hand, reactive power injections occur mainly during periods of lower active power generation. The higher reactive power at node 707 also indicates that more commercial customers are closer to it.

Figure 7 depicts the maximum decrease in apparent power of inverters and the comparison of empirical probabilities of apparent power violations (including both PV facilities) with the (deterministic) mixed-integer linear programming (MILP) model. For the empirical probabilities, the case study uses 720 new random samples of forecast errors each hour obtained from a Monte Carlo simulation. The decrease in apparent power reaches the presented highest values at 15:00 for both nodes. Likewise, the empirical probabilities (represented by the color dots) indicate numerous apparent power violations with the MILP model that significantly exceed the acceptable limit (represented by the black horizontal lines). In contrast, only a few constraints have slightly higher empirical probabilities using the MISOCP model.

However, considering the uncertainty leads to an increase in the DSO's expected cost. For March 6, this cost corresponds to $15.1 using the MILP model and $50.3 using the MISOCP model. Furthermore, this value depends on the level of PV generation. For example, Table III presents several scenarios with different percentages of the initial PV generation depicted in Fig. 2, maintaining the same market price. While expanding the PV capacity yields a profit (remarkably higher in the scenario with 200% of the initial PV generation), the absence of PV facilities results in a high daily cost unless adjustments to the bounds of decision prices occur. Specifically, in simulations with 120%, 150%, and 200% of

the initial PV generation, the apparent power of inverters also increases proportionally.

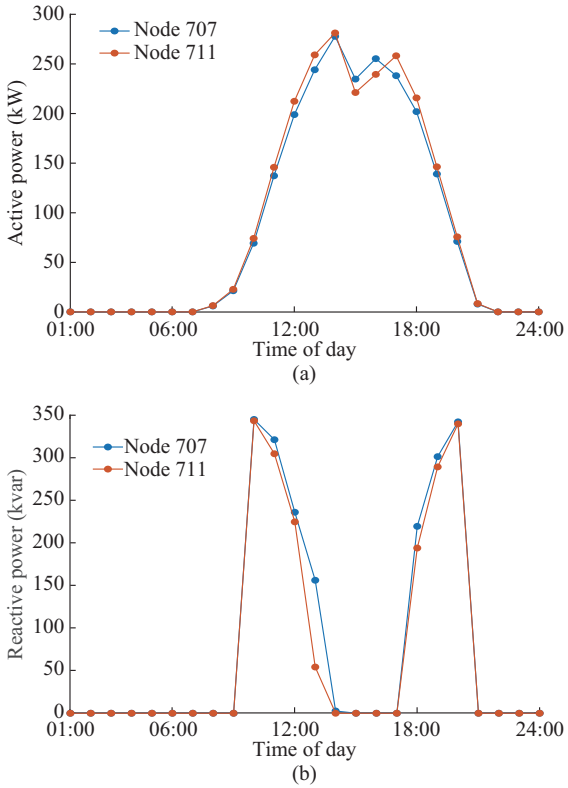

Fig. 6. Active and reactive power set points of PV facilities at nodes 707 and 711 on March 6. (a) Active power. (b) Reactive power.

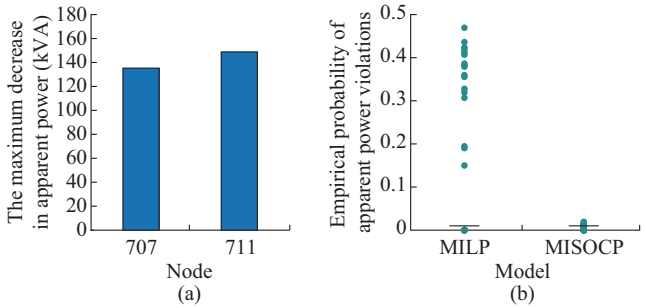

Fig. 7. The maximum decrease in apparent power of inverters and comparison of empirical probabilities of apparent power violations with MILP and MISOCP models. (a) The maximum decrease in apparent power of inverters. (b) Comparison of empirical probabilities of apparent power violations.

TABLE III
SCENARIOS WITH DIFFERENT PERCENTAGES OF INITIAL PV GENERATION

Percentage (%)	DSO's expected profit ($)	DSO's expected cost ($)
120	38.1	
150	182.3	
200	403.4	
80		117.4
50		264.3
0		528.3

Finally, the case study assesses the impact of uncertainty by considering the voltage at extreme node 741 under the condition of PV facilities connected to the main branch. Node 741 experiences the highest voltage drops when the PV facilities are, for instance, at nodes 702 and 709. Using this connection, Fig. 8 shows the expected voltage at node 741 obtained with the MILP and MISOCP models for the critical time of 19:00, including the CDF of voltage deviations superimposed. Due to incorporating uncertainty in the MISOCP model, the squared voltage increases to 20.91 kV^2. This increment represents a reduction in the probability of constraint violation from close to 30% with the MILP model to the established 10% with the MISOCP model. With the new configuration, the DSO's expected cost is $54.8.

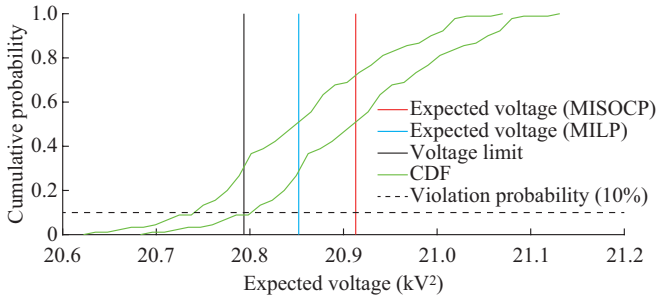

Fig. 8. Expected voltage at node 741 obtained using MILP and MISOCP models for the critical time of 19:00.

B. Case Study II

For simplicity, this case study presents only the customized price signals according to each highest-probability RPC on March 13, the expected consumption profiles, and the active and reactive power set points of PV facilities. As in case study I, three clusters characterize customers' behavior during the corresponding three weeks. The shapes of these clusters are very similar to those in Fig. 3 due to the closeness of both measurement periods. Table IV summarizes the three RPCs, their combinations, and the number of customers associated with each highest-probability RPC on March 13. Most consumers use a combination of RPCs 1 and 2 (72.9% of the total), and the DSO primarily expects the RPC 2.

TABLE IV
RPCS, THEIR COMBINATIONS, AND NUMBER OF CUSTOMERS PER HIGHEST-PROBABILITY RPC ON MARCH 13

RPC	Number of customers	Combination of RPCs (number of customers in corresponding combination)	Number of customers per highest-probability RPC on March 13
1	64	2 (41), 1 (20), 3 (3)	108
2	315	1-2 (306), 1-3 (4), 2-3 (5)	302
3	41	1-2-3 (41)	10

The customized price signals according to each highest-probability RPC on March 13 are depicted in Fig. 9. In the customized price signal according to RPC 1, the minimum price (60 $/MWh) is uniform except from 22:00 to 23:00. This result encourages customers with RPC 1 to shift their higher consumption at night to close hours in the afternoon, coinciding with lower market prices and higher PV genera-

tion. A different situation characterizes the customized price according to RPC 2, where the minimum price ranges mainly from 13:00 to 21:00, involving most of the daily demand of customers with RPC 2. The DSO minimizes costs if these consumers maintain a higher consumption during this period. Finally, customers with RPC 3 face a significant challenge because the customized price signal according to RPC 3 requires them to change their consumption pattern on the test day. In particular, periods of higher consumption (from the beginning of the day to 09:00 and at the end of the day) coincide with higher market prices.

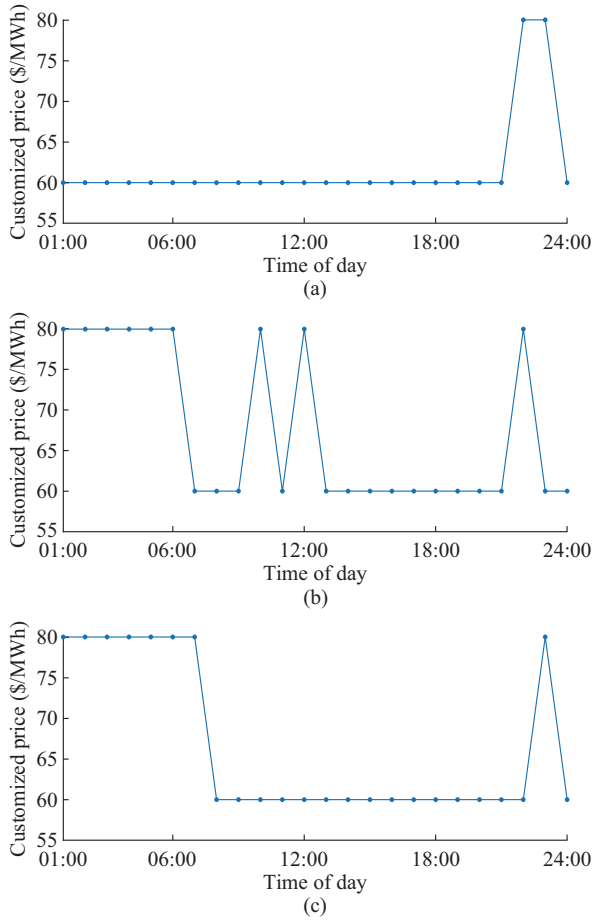

Fig. 9. Customized price signals according to highest-probability RPC on March 13. (a) RPC 1. (b) RPC 2. (c) RPC 3.

Figure 10 depicts the expected consumption profiles of customers, where the black profile represents the average consumption. A similar consumption pattern characterizes customers with RPCs 1 and 2, with notably higher demand from 13:00 to 19:00. This period involves high PV generation and low market prices. Customers with RPC 2, however, have higher consumption than those with RPC 1. This result also demonstrates the high flexibility of both in shifting consumption according to the DSO's price signals. Concerning customers with RPC 3, they reduce their demand in the early morning and at night.

Finally, Fig. 11 illustrates the active and reactive power set points of PV facilities, which exhibit similar behavior as those in Fig. 6. The differences (in the corresponding values) arise from the specific grid conditions on the selected dates. In particular, March 13 implies an expected profit of $235.4 for the DSO.

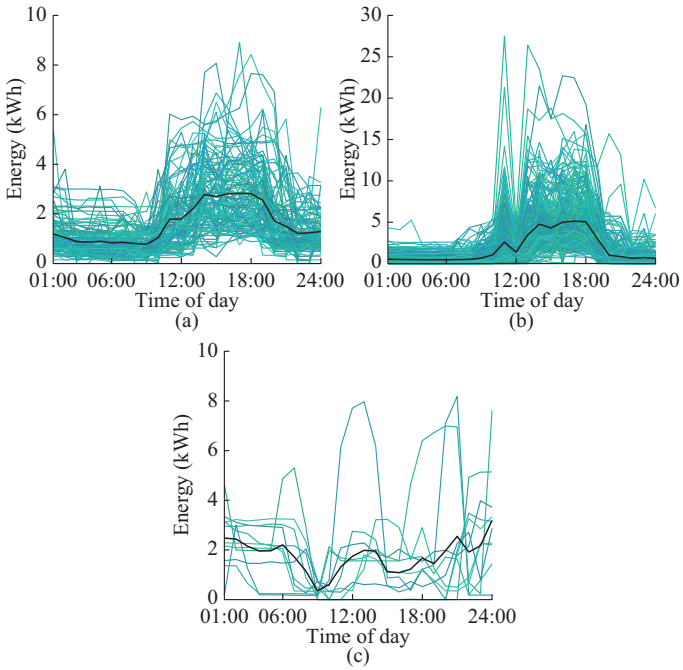

Fig. 10. Expected consumption profiles of customers on March 13. (a) RPC 1. (b) RPC 2. (c) RPC 3.

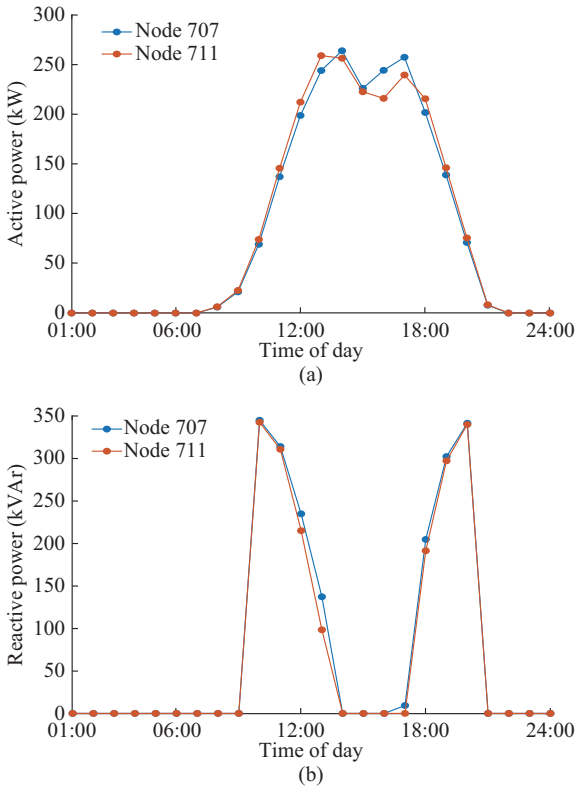

Fig. 11. Active and reactive power set points of PV facilities at nodes 707 and 711 on March 13. (a) Active power. (b) Reactive power.

C. Comparison Analysis

Supplying electricity to customers through customized tar-

iffs provides technical and economic benefits for the DSO. In contrast, implementing a uniform price signal overlooks the specific preferences of individual customers.

Figure 12 depicts the uniform price signals to be broadcast by the DSO on March 6 and March 13. Both price signals are derived based on the specific characteristics defined for the case studies. A comparison of these price signals with Figs. 4 and 9 reveals two significant issues: ① the shape of the resulting uniform price scheme exhibits very few changes; and ② in general, the most prevalent RPCs of customers are reflected in the uniform price signals. For instance, on March 6, the price signal maintains the minimum price (60 $/MWh) until noon, which aligns with the profile obtained for customers with RPC 1 in Fig. 4. After noon, the shape of the price signal matches that for customers with RPC 2. Similarly, on March 13, the minimum price is observed before 09:00, while the rest of the day resembles the price signal for customers with RPC 2. Thus, these tariffs do not adequately consider customers with RPC 3, while the representation of the other two RPCs is partial.

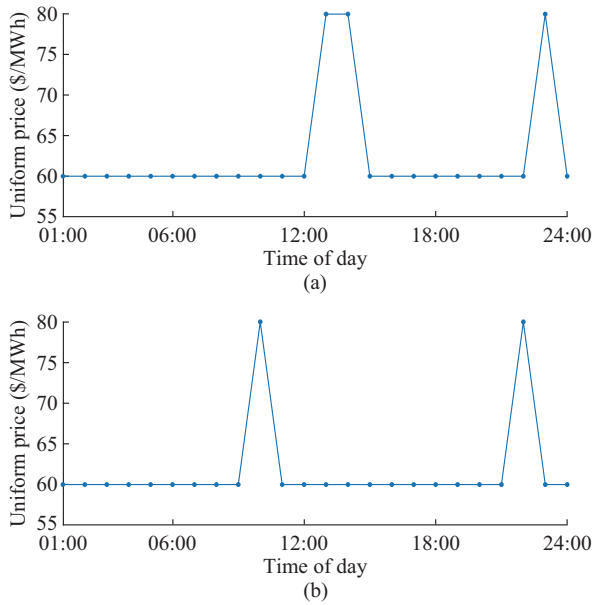

Fig. 12. Uniform price signals to be broadcast by DSO on March 6 and March 13. (a) March 6. (b) March 13.

On the other hand, the total cost for the DSO on March 6 is $64.4, which is higher than the cost incurred using the proposed approach ($50.3). Similarly, the DSO records a profit of $207.6 on March 13, which is lower than the profit obtained using the proposed approach ($235.4). As a result, the cost minimization achieved through the uniform price scheme is less effective, which is a finding that aligns with the conclusion presented in [13].

VI. Conclusion

This paper presents a customized scheduling approach for DR of customers with dispatchable inverters in distribution-level PV facilities. Providing flexibility by scheduling the demand side supports the DSO in the technical and economic management of the distribution system. Specifically, the DSO minimizes distribution system costs by determining daily price signals for customers based on their RPCs and active and reactive power set points for PV facilities. Furthermore, the proposed approach ensures the reliable operation of the distribution system with high probability by addressing uncertainty through CCs.

The conducted case studies use real-world market prices and daily consumption profiles of residential and commercial Chilean customers on the IEEE 37-node test feeder. Results highlight the suitability of the proposed model to manage distribution-level energy resources by delivering customized price signals and power set points, respectively. The proposed approach provides an expected cost for the DSO; however, the DSO has the final decision concerning the tradeoff between the security and cost in the distribution system.

The proposed approach can be extended, for example, by including maximum ramp rates in the customer model, a higher number of PV facilities or other distribution-level energy resources, and different risk levels (measured in CCs in terms of the violation probability) and probability distributions for deviations and errors.

Future work will expand this investigation by addressing two significant issues: ① analysis of the unbalanced distribution system with DR and other distributed energy resources; and ② an online application of the scheduling problem to account for updated information on system parameters.

References

[1] National Energy Commission. (2024, Nov.). National energy balance. [Online]. Available: http://energiaabierta. cl/visualizaciones/balance-de-energia

[2] J. S. Vardakas, N. Zorba, and C. V. Verikoukis, "A survey on demand response programs in smart grids: pricing methods and optimization algorithms," *IEEE Communications Surveys & Tutorials*, vol. 17, no. 1, pp. 152-178, Jan. 2015.

[3] M. Tanaka, A. J. Conejo, and A. S. Siddiqui, *Economics of Power Systems*. Cham: Springer, 2022.

[4] D. T. Nguyen, H. T. Nguyen, and L. B. Le, "Dynamic pricing design for demand response integration in power distribution networks," *IEEE Transactions on Power Systems*, vol. 31, no. 5, pp. 3457-3472, Sept. 2016.

[5] H. Karimi, R. Bahmani, and S. Jadid, "Stochastic multi-objective optimization to design optimal transactive pricing for dynamic demand response programs: a bi-level fuzzy approach," *International Journal of Electrical Power & Energy Systems*, vol. 125, p. 106487, Feb. 2021.

[6] V. C. Pandey, N. Gupta, K. R. Niazi *et al*., "A hierarchical price-based demand response framework in distribution network," *IEEE Transactions on Smart Grid*, vol. 13, no. 2, pp. 1151-1164, Mar. 2022.

[7] H. J. Monfared and A. Ghasemi, "Retail electricity pricing based on the value of electricity for consumers," *Sustainable Energy, Grids and Networks*, vol. 18, p. 100205, Jun. 2019.

[8] M. Askeland, T. Burandt, and S. A. Gabriel, "A stochastic MPEC approach for grid tariff design with demand-side flexibility," *Energy Systems*, vol. 14, no. 3, pp. 707-729, Aug. 2023.

[9] Q. Cai, Q. Xu, J. Qing *et al*., "Promoting wind and photovoltaics renewable energy integration through demand response: dynamic pricing mechanism design and economic analysis for smart residential communities," *Energy*, vol. 261, p. 125293, Dec. 2022.

[10] Y. Tao, J. Qiu, S. Lai *et al*., "Customer-centered pricing strategy based on privacy-preserving load disaggregation," *IEEE Transactions on Smart Grid*, vol. 14, no. 5, pp. 3401-3412, Sept. 2023.

[11] S. Su, Z. Li, X. Jin *et al*., "Bi-level energy management and pricing for community energy retailer incorporating smart buildings based on chance-constrained programming," *International Journal of Electrical Power & Energy Systems*, vol. 138, p. 107894, Jun. 2022.

[12] F. Meng, Q. Ma, Z. Liu *et al*., "Multiple dynamic pricing for demand response with adaptive clustering-based customer segmentation in

smart grids," *Applied Energy*, vol. 333, p. 120626, Mar. 2023.
[13] D. Qiu, Y. Wang, J. Wang *et al*., "Personalized retail pricing design for smart metering consumers in electricity market," *Applied Energy*, vol. 348, p. 121545, Oct. 2023.
[14] P. Che, C. Zhang, Y. Liu *et al*., "An integrated learning and optimization approach to optimal dynamic retail electricity pricing of residential and industrial consumers," *Applied Energy*, vol. 382, p. 125234, Mar. 2025.
[15] Chilean Association for Renewable Energies and Storage. (2025, Mar.). Information center. [Online]. Available: https://www.acera.cl/centro-de-informacion
[16] E. Dall'Anese, K. Baker, and T. Summers, "Chance-constrained AC optimal power flow for distribution systems with renewables," *IEEE Transactions on Power Systems*, vol. 32, no. 5, pp. 3427-3438, Sept. 2017.
[17] M. Rayati, M. Bozorg, R. Cherkaoui *et al.*, "Distributionally robust chance constrained optimization for providing flexibility in an active distribution network," *IEEE Transactions on Smart Grid*, vol. 13, no. 4, pp. 2920-2934, Jul. 2022.
[18] T. Ding, C. Li, Y. Yang *et al*., "A two-stage robust optimization for centralized-optimal dispatch of photovoltaic inverters in active distribution networks," *IEEE Transactions on Sustainable Energy*, vol. 8, no. 2, pp. 744-754, Apr. 2017.
[19] J. M. Morales, A. J. Conejo, H. Madsen *et al.*, *Integrating Renewables in Electricity Markets: Operational Problems*. New York: Springer, 2014.
[20] S. A. Gabriel, A. J. Conejo, J. D. Fuller *et al.*, *Complementarity Modeling in Energy Markets*. New York: Springer, 2013.
[21] L. Marrero, D. Sbarbaro, and L. Garcia-Santander, "Online demand response characterization based on variability in customer behavior," *Journal of Modern Power Systems and Clean Energy*, vol. 12, no. 3, pp. 936-946, May 2024.
[22] D. Bienstock, M. Chertkov, and S. Harnett, "Chance-constrained optimal power flow: risk-aware network control under uncertainty," *SIAM Review*, vol. 56, no. 3, pp. 461-495, Jan. 2014.
[23] Ministry of Energy, National Energy Commission. (2023, Nov.). Resolution 574 exempt. [Online]. Available: https://www. bcn. cl/leychile/navegar?idNorma=1198390
[24] A. Rodriguez and A. Laio, "Clustering by fast search and find of density peaks," *Science*, vol. 344, no. 6191, pp. 1492-1496, Jun. 2014.
[25] *IEEE Standard for Interconnection and Interoperability of Distributed Energy Resources with Associated Electric Power Systems Interfaces*, IEEE Standard 1547-2018, Apr. 2018.
[26] M. E. Baran and F. Wu, "Optimal capacitor placement on radial distribution systems," *IEEE Transactions on Power Delivery*, vol. 4, no. 1, pp. 725-734, Jan. 1989.
[27] R. Sioshansi and A. J. Conejo, *Optimization in Engineering: Models and Algorithms*. Cham: Springer, 2017.
[28] M. S. Nazir, I. A. Hiskens, A. Bernstein *et al.* (2019, Mar.). Inner approximation of Minkowski sums: a union-based approach and applications to aggregated energy resources. [Online]. Available: https://www.nrel.gov/docs/fy19osti/73423.pdf
[29] J. Fortuny-Amat and B. McCarl, "A representation and economic interpretation of a two-level programming problem," *Journal of the Operational Research Society*, vol. 32, no. 9, pp. 783-792, Sept. 1981.
[30] GitHub. (2024, Dec.). YALMIP. [Online]. Available: https://yalmip.github.io
[31] IEEE. (2017, Sept.). IEEE PES test feeder. [Online]. Available: https://cmte.ieee.org/pes-testfeeders/resources
[32] A. Molina, M. Falvey, and R. Rondanelli, "A solar radiation database for Chile," *Scientific Reports*, vol. 7, no. 1, p. 14823, Dec. 2017.

Lester Marrero received the B.Sc. and M.Sc. degrees in electrical engineering from Universidad Central de Las Villas, Santa Clara, Cuba, and the Ph.D. degree in electrical engineering from Universidad de Concepción, Concepción, Chile, in 2024. He is currently a Postdoctoral Researcher at the Center for Energy Transition, Universidad Adolfo Ibáñez, Santiago, Chile. His research interests include modeling and optimization of electric distribution systems, distributed energy resources, and data analytics in smart grids.

Daniel Sbárbaro received the electrical engineering degree from Universidad de Concepción, Concepción, Chile, in 1984, and the Ph. D. degree in electrical engineering from Glasgow University, Glasgow, U.K., in 1993. In 1998, he was an Alexander von Humboldt Fellow with the Control Engineering Laboratory, Ruhr University, Bochum, Germany. He also held Visiting Research positions with the Daimler-Benz Research Institute, Berlin, Germany, and Stuttgart University, Stuttgart, Germany, in 1993 and 2009, respectively. He has developed projects with the industry in the areas of technological benchmarking, economic assessment of control improvements, development of training programs, advanced control, and data processing. He is currently a Professor with the Department of Electrical Engineering, Universidad de Concepción. His current research interests include modeling and control of energy systems and development of technologies for improving sustainability of main Chilean productive sectors.

Luis García-Santander received the Ph. D. degree in electrical engineering from Supélec, Paris, France, in 2003. Since 1996, he has been with the Department of Electrical Engineering, Universidad de Concepción, Concepción, Chile, where he is currently an Associate Professor. His research interests include renewable generation, planning and operation of distribution systems, energy management and efficiency, smart grid, and electromobility.